Electrochimica Acta 548 (2026) 147985

Contents lists available at ScienceDirect

Electrochimica Acta

journal homepage: www.journals.elsevier.com/electrochimica-acta

A practical approach to thickness-dependent cell constant correction for coplanar or interdigitated electrodes

Max Stevenson [a,b], Michael König [a], Ina Klein [a], Radha Boya [c], Jürgen Senker [a,b], Markus Retsch [a,b], Josef Breu [a,b,*]

[a] Department of Chemistry, University of Bayreuth, Universitätsstraße 30, 95447 Bayreuth, Germany
[b] Bavarian Center for Battery Technology (BayBatt), University of Bayreuth, Universitätsstraße 30, 95447 Bayreuth, Germany
[c] Department of Physics & Astronomy, University of Manchester, M13 9PL, United Kingdom

ARTICLE INFO

Keywords:
Interdigitated electrode
Cell constant
Correction factor
Film thickness, EIS

ABSTRACT

Coplanar microelectrodes, particularly interdigitated electrodes (IDEs), are widely employed in electrochemical sensing owing to low cost, scalable fabrication, and high surface sensitivity. However, accurate and quantitative interpretation requires precise determination of the cell constant (k). This becomes nontrivial when the electrode's electric field is only partially immersed in the electrolyte, as is common in thin film or confined-volume systems. This work presents a fast, reproducible, and low-cost experimental platform for measuring film thickness-dependent correction factors (α) of k. Electrochemical impedance spectroscopy (EIS) was applied on printed circuit board (PCB) IDEs comprising five different electrode finger widths (w) and spacings (s) ($w = s$: 250 µm, 500 µm, 1000 µm, 1500 µm, and 2000 µm). k was determined while fully immersed, and α was subsequently empirically derived as a function of electrolyte film thickness ($\alpha(d)$). The results were compared to finite element methods (FEM; COMSOL), revealing consistent trends but notable deviations in absolute values of $\alpha(d)$. These findings highlight the limitations of simplified field models and provide a practical approach for a more accurate characterization of thin films on coplanar electrodes.

1. Introduction

Interdigitated electrodes (IDE) are a highly attractive platform as sensors [1,2], clinical bioelectronics [3–8], or for the electrochemical analysis [1–3] of thin film interfacial and bulk transport properties. Simple and scalable manufacturing processes, such as screen printing[4] or printed circuit board (PCB) fabrication [5,6], enable devices that can be readily integrated into various environments and configurations[7]. Furthermore, the sensitivity range is determined by the electrode dimensions[8], which can be tailored to investigate bulk material properties[9], determine single crystal properties [10,11], or detect trace levels of analytes [12,13]. The sensitivity is affected by the number of electrode fingers in the array (N), the electrode lengths (L), and the electrode finger widths (w) and spacings (s)[14], with array sizes ranging from nanometers [15,16] to several centimeters[17]. This flexibility makes IDEs the perfect toolkit to investigate processes across various timescales and material loadings.

An essential characteristic constant of any electrochemical setup, including IDEs, is the cell constant k [cm^{-1}], which allows for the conversion of the measured resistance R [Ω] to the material-specific conductivity σ [µS cm^{-1}] (Fig. 1)[8]. It describes the dimension of the electric field and allows for the geometric normalization of the measured current density (j) and R. k of typical parallel plate setups (Fig. 1a) in electrochemical impedance spectroscopy (EIS) is simply defined by $d_{Parallel}/A$, which is the distance between the electrode plates ($d_{Parallel}$) and the area of the plate electrode (A). In the case of coplanar electrode designs, determining k is more sophisticated and must be differentiated for two distinct setups (Fig. 1b and c). As the electrode dimension of a manufactured IDE is fixed, k is a constant whenever the electric field of the IDE is fully immersed within a material (Fig. 1b). k is determined in advance by immersing the electrode in an electrolyte solution of known σ, measuring R, and utilizing the relation $k = \sigma^* R^{-1}$. If the electric field of the IDE is not fully immersed, e.g., by a deposited thin film, k must be adjusted by a correction factor α (Fig. 1c) [18]. α describes the relationship between deposited film thickness (d) and R. It ensures that σ remains consistent across films of varying d, as R varies with d.

* Corresponding author.
E-mail address: Josef.Breu@uni-bayreuth.de (J. Breu).

https://doi.org/10.1016/j.electacta.2025.147985
Received 6 October 2025; Received in revised form 28 November 2025; Accepted 8 December 2025
Available online 8 December 2025

This relationship was previously estimated[18] applying finite element method simulations (FEM; COMSOL) of the coplanar electrodes repeat unit for different film thicknesses. j was extracted as a function of film thickness $j(d)$, and α as a function of film thickness $\alpha(d)$ was obtained by normalization to a maximum of $\alpha = 1$. Applying the relation of $\sigma = k^*R^{-1}*\alpha(d)^{-1}$ allows for converting R to the corresponding material-specific σ at any d. The simulation results were validated by comparing them with experimental measurements obtained from screen-printed films on IDEs, using a reference material of known conductivity and thin films of varying thickness. While this is a valid theoretical and experimental method, the characterization procedure requires specific equipment, is rather time-consuming and expensive, and the results cannot be generalized for other coplanar dimensions. This work presents an experimental, reproducible, simple, low-cost, and time-efficient method to determine $\alpha(d)$.

2. Materials and methods

2.1. Definitions and working equations

Fully immersed calibration $d \to \infty$ defines the cell constant $k = \sigma R(\infty)$ via the measured resistance $R(\infty)$ and known electrolyte conductivity σ.

For a film of thickness d, with measured resistance $R(d)$, we define the thickness correction factor $\alpha(d) = R(\infty)/R(d)$ [$0 < \alpha(d) \leq 1$, and $\alpha(d) \to 1$ for $d \to \infty$].

Unless otherwise stated, R is extracted as the resistive plateau of the Bode magnitude $|Z|$ (e.g., 10 kHz for the electrolytes and geometries studied). Because the entire $|Z|$ plateau corresponds to the resistivity of the ionic conduction process, any frequency within this frequency region yields the same $\alpha(d)$, and the precise choice of frequency does not influence the extracted correction factor.

The working equation used throughout to obtain σ from a thin film measurement is $\sigma = kR(d)^{-1}\alpha(d)^{-1}$.

For the FEM simulations, $\alpha(d)$ was defined from the simulated current density $j(d)$ by normalization, $\alpha(d) = j(d)/j(\infty)$ [$0 < \alpha(d) \leq 1$, and $\alpha(d) \to 1$ for $d \to \infty$]. Note that this normalization differs from the experimental definition, where $\alpha(d)$ is obtained as the reciprocal ratio of R.

2.2. Materials and methods

Conductivity standards ROTI®Calipure (aqueous KCl, 84 µS cm^{-1}, 500 µS cm^{-1}, 1413 µS cm^{-1} at 25 °C; Carl Roth, Germany), PLA Filament (Prusa, Poland), and the electronic micrometer were used as received (RS-PRO, United Kingdom; Resolution: ±1 µm, Accuracy: ±4 µm). PCB IDEs (JLC-PCB, China) were selected for this work due to their cost-efficiency, manufacturing precision, availability in large quantities, and a wide range of dimensions. The electrode fingers (copper traces) were protected from corrosion by a 2 µin ENIG coating (Nickel-Gold). EIS was measured on a Novocontrol Alpha-A Mainframe equipped with a ZG4 module in a frequency range of 10 MHz to 100 Hz at an excitation voltage of 10 mV. COMSOL Multiphysics (Version 6.2) was used for FEM simulations. Custom-built components were printed by a Prusa XL. CLSM was carried out with a LEXT OLS5000 Olympus 3D laser scanning microscope.

2.3. Cell constant determination

IDEs were placed into the custom-built container (Fig. S1) and fully immersed in conductivity reference solutions (σ: 84 µS cm^{-1}, 500 µS cm^{-1}, 1413 µS cm^{-1}). EIS was measured in a frequency range of 10 MHz to 100 Hz at an excitation voltage of 10 mV. Three electrodes of each IDE type were immersed in each of the conductivity standards, and the cell constant was determined as the mean of all measurements. Electrodes originating from the same fabrication batch consistently yielded nearly identical cell constants, demonstrating the high reproducibility of the PCB-manufactured IDEs. Throughout all measurements, the temperature of the conductivity standards was monitored to ensure correct referencing of their specified conductivities.

2.4. Correction factor determination

An IDE and a flat, non-conductive, sandpaper-polished PLA disk were fixed to opposing sides of a micrometer screw in a parallel arrangement with a tight slip fit (Clearance of 0.1 mm). With the components mounted, the micrometer screw was initially tightened by hand to ensure a proper fit of the mounted parts. Gently retightening the micrometer screw with the ratchet stop (5–10 N) and setting the display to 0 µm allowed for a reproducible control (±5 µm, Fig. S2) of the distance (d_{Setup}) between the flat PLA disk and the electrode traces of the

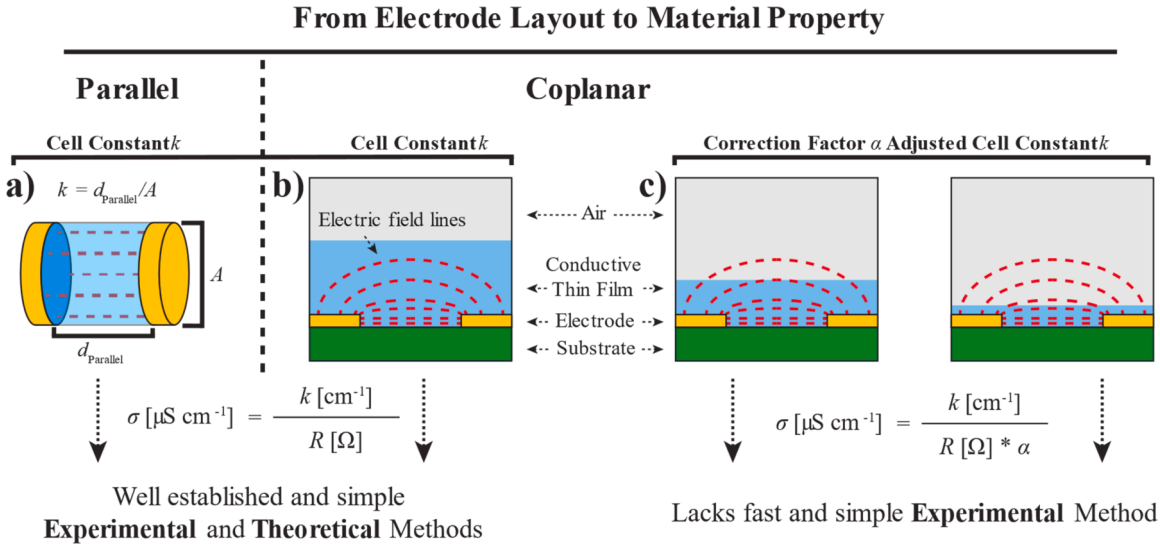

Fig. 1. Schematic of the a) parallel and b) coplanar electrode layout with illustrative electric field lines. k of parallel plate setups is always $d_{Parallel}/A$, while k of coplanar layouts must be determined experimentally. c) When a conductive film (blue) does not fully immerse the electric field of the coplanar electrodes, k must be adjusted by α to convert the measured R to the material-specific σ. α is film thickness (d) dependent.

IDE. A starting distance of $d_{Initial} = 6000$ μm was set for every IDE type. The electrolyte solution was carefully added to fill the space between the IDE and the opposing disk while avoiding bubbles. EIS was recorded for 20–50 distances by adjusting the micrometer screw. As the micrometer screw measures the distance between the PLA disk and the electrode traces (not the electrode substrate), d was calculated as $d = d_{Setup}+h$, where h describes the electrode trace height above the IDE-substrate of $h = 33$ μm.

2.5. Finite element method comsol

FEM simulations were performed with the software COMSOL Multiphysics (Version 6.2). The experimental setup was designed to be true to scale in COMSOL, and the material properties provided by the software were assigned to the corresponding parts of the setup. Current conservation was ensured for all parts. The electric potential of one electrode was set to 10 mV, and the other electrode was grounded. The boundaries of all remaining parts were electrically insulated from the surroundings of the setup. The normalized electric field and current density were simulated for varying d (1 μm - 10,000 μm), $w = s$ (250 μm, 500 μm, 1000 μm, 1500 μm, and 2000 μm), and an electrode height (h) of 33 μm. All datasets were obtained using parametric sweeps.

3. Results

For this work, we chose five different electrode dimensions with $w = s$ of 250 μm, 500 μm, 1000 μm, 1500 μm, and 2000 μm (Table 1 and Fig. 2a). To determine k (Table 1, Figs. 2b and S1a), each IDE type was immersed in three different conductivity standard solutions (σ: 84 μS cm^{-1}, 500 μS cm^{-1}, 1413 μS cm^{-1}) and EIS was measured in a frequency range of 10 MHz to 100 Hz at an excitation voltage of 10 mV.

The frequency of the ionic process shifts towards higher frequencies for electrolytes of higher conductivity, which is indicated by the shifted maximum of φ in the Bode plot (Fig. 2c). At low frequencies, the electrode polarisation of adjacent electrode fingers is indicated by a low-frequency decrease of φ in the Bode plot and a low-frequency tail in the Nyquist plot (Fig. 2d). When comparing the Bode (Fig. 2e) and Nyquist plots (Fig. 2f) of different IDE types, the frequency of the ionic process is unaffected by the IDE type and only affected by the electrolyte's conductivity. Furthermore, the trend of R as a function of IDE-type is in accordance with prior works by Olthuis et al.[8], where a smaller w resulted in a smaller R and, therefore, a smaller k.

3.1. Experimental determination of α(d)

The experimental determination of $\alpha(d)$ (Fig. 3) involves an IDE and a flat non-conductive polylactic acid (PLA) disk (Figs. 3a and S1b). The details of the experimental procedure can be found in the experimental section (Section 2.4). R was extracted as $|Z|$ at 10 kHz. With an initial d of $d_{Initial} = 6000$ μm, $R(d)$ matched each IDE type's fully immersed R values. An identical R of both setups prevents a faulty normalization and is thus a prerequisite for determining $\alpha(d)$. By adjusting the micrometer screw, EIS was recorded for 20–50 distances. An increasing R with decreasing d (Fig. 3b) is expected as conductive volume is removed stepwise. A change in the frequency of the ionic process is not expected, as the material's specific conductivity (84 μS cm^{-1}) and mobility of the ionic species are not affected by varying electrolyte film thickness. This is confirmed by the maximum of φ (Fig. 3c Top) and the plateau of $|Z|$ (Fig. 3d Bottom) being invariant of the frequency. $\alpha(d)$ is determined by extracting R as a function of d and reciprocally normalizing $R(d)$ to a maximum of $\alpha(d_{Initial}) = 1$ (Fig. 3d). With the results of $\alpha(d)$, σ of a thin film on an IDE is obtained by the relation of $\sigma = kR(d)^{-1}\alpha(d)^{-1}$. Exner et al.[18] observed three regimes for $\alpha(d)$: regime (I) with a linear increase of α at small d ($d < 50\ \% * w$), followed by (II) a non-linear transition regime at medium d ($50\ \% < d < 200\ \% * w$), before (III) a plateau of $\alpha = 1$ at large d ($200\ \% * w < d$). The same three regimes were observed for our method of determining $\alpha(d)$.

Table 1
IDE type, w & s, h, L, N, and k.

IDE type	w & s	h	L	N	k [cm^{-1}]
250 μm	250 μm	33 μm	17 mm	21	0.041 ± 0.001
500 μm	500 μm	33 μm	17 mm	11	0.090 ± 0.004
1000 μm	1000 μm	33 μm	17 mm	6	0.166 ± 0.010
1500 μm	1500 μm	33 μm	17 mm	4	0.262 ± 0.011
2000 μm	2000 μm	33 μm	17 mm	3	0.353 ± 0.023

3.2. Comparison with FEM simulations

$\alpha(d)$ was determined multiple times for all IDE types (Table 1), yielding consistent results. Simultaneously, $\alpha(d)$ was simulated using FEM (COMSOL) by modelling the repeat unit of each IDE type (Fig. 4a) and extracting j while varying d. Experiment and simulation results (Fig. 4b and c) accurately capture the trend of decreasing IDE size. However, the actual values of $\alpha(d)$ differ substantially, especially at smaller d. The overall experimental $\alpha(d)$ in the linear regime (I) at smaller d ($d < 100\ \% * w$) is much higher than the FEM determined value. Furthermore, the transition regime (II) appears at a smaller d compared to the simulation. At large d of regime (III) ($d > 150\ \% * w$), the results for $\alpha(d)$ of both methods align again.

There are multiple possible reasons for the deviations of $\alpha(d)$ of the experimental data and the simulation, two of which appear to be most relevant in the context of this study: The simplified two-dimensional (2D) simulation cannot fully capture the electric field line fringes of the IDE, as the fabricated structures feature non-idealities such as rounded corners, angled and microscopically rough surfaces, and field curvature around individual electrode fingers. Furthermore, FEM solves the same governing equations for each simulation, ignoring array sizes. This oversimplification becomes evident when d is normalized by the respective w of each simulated IDE-type (Fig. 4d), where all simulated $\alpha(d)$ collapse onto a single curve. On the other hand, when determining $\alpha(d)$ for the real IDE, variations in w, s, h, L, and N and their effect on the electric field are implicitly accounted for. In this study, a larger N with a smaller w deviates from the simulated trend to a larger extent, suggesting that these arrays are more affected by fringing effects. In theory, these fringes should be compensated for by long electrode fingers; however, in the scope of this study, the exact extent of fringing was not explicitly determined.

3.3. Downsizing array dimensions

Alternatively, the deviations of experimentally determined and FEM simulated $\alpha(d)$ in regime (I) may be minimized by down-sizing electrode arrays. For this, another smaller IDE array with identical $w = s = 500$ μm, but smaller $L = 5.5$ mm and $N = 8$ (Table 2, Fig. 5a) was investigated, and $\alpha(d)$ was compared to the experimental and simulation results of the larger 500 μm IDE-type (Fig. 5b). For the smaller array and its simulation, $\alpha(d)$ aligns with the simulation results at small d in regime (I) but deviates at larger d in regime (II). Furthermore, despite identical w, s, and h, the experimental $\alpha(d)$ of the small and large arrays are not identical, which we attribute to the shorter finger length as it introduces a different proportion of fringe-field contributions, which becomes relevant in regime (II). When comparing $\alpha(d)$ of the two dimensions, it becomes evident that even though the results of FEM are valid for some film-thickness ranges of each array, they cannot be generalized for all array dimensions purely based on w, s, and h. Thus, additional empirical methods are required to fully capture the effects of array dimensions and accurately characterize material properties. As the proposed experimental determination of $\alpha(d)$ is simple and as fast as FEM simulation, it clearly is the preferred approach to determine $\alpha(d)$ for a broader range of d.

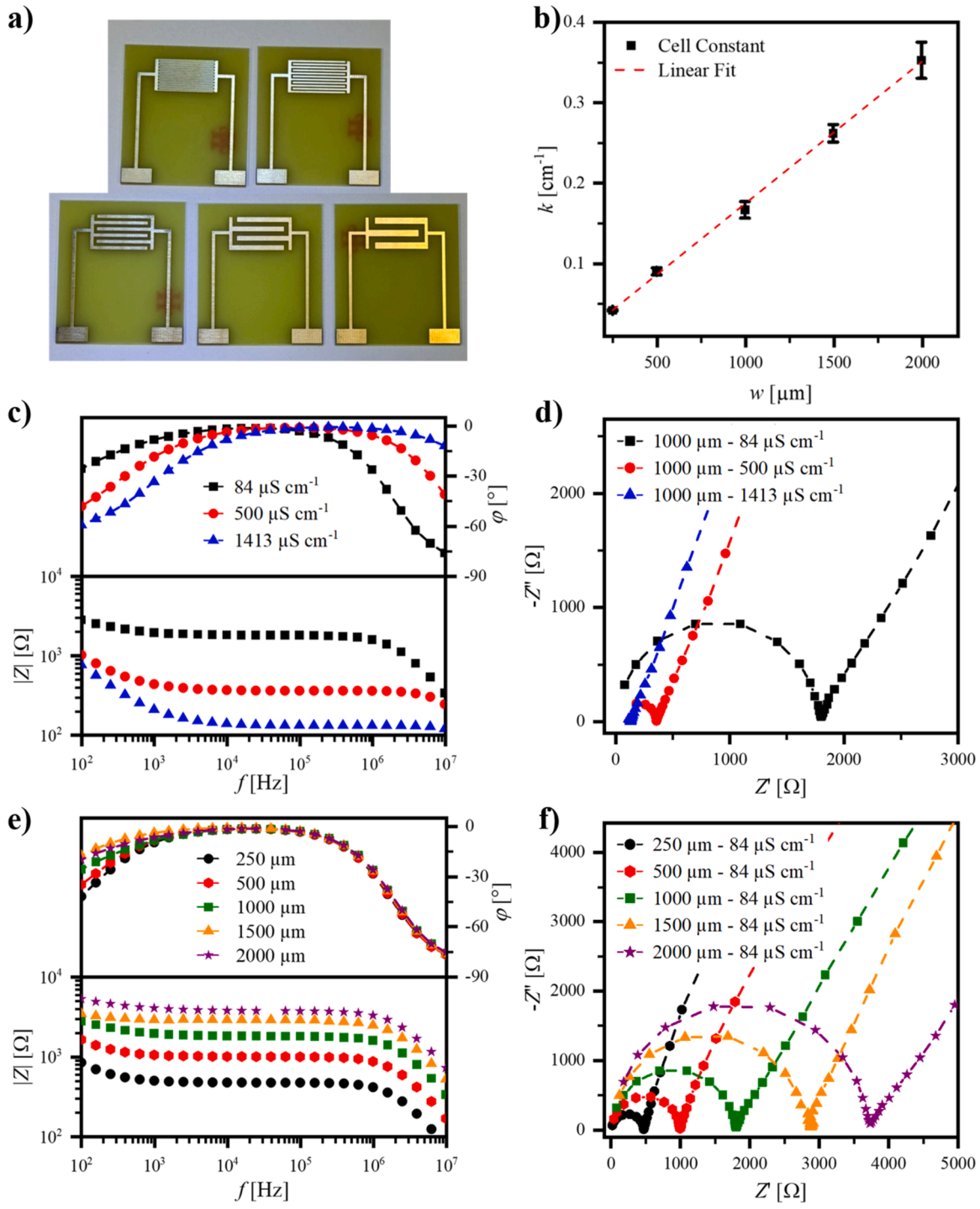

Fig. 2. a) Digital picture of the different IDE types with $w = d$ of 250 µm, 500 µm, 1000 µm, 1500 µm, and 2000 µm. b) k of the different IDE types. Exemplary c) Bode (Top: Phase angle (φ); Bottom: Magnitude $|Z|$) and d) Exemplary Nyquist plot of the 1000 µm IDE-type when fully immersed in three different conductivity standards (84 µS cm^{-1}, 500 µS cm^{-1}, 1413 µS cm^{-1}). Exemplary e) Bode (Top: φ; Bottom: $|Z|$) and f) Nyquist plot of the different IDE types when fully immersed in the 84 µS cm^{-1} conductivity standard. In c)-f) dashed lines were added for visual clarity and do not indicate refined models.

3.4. Controls and artefact checks

The authors would like to highlight three additional factors that may seem plausible but did not contribute to the deviations between the simulation and the experiments.

Firstly, insufficient electrolyte coverage (in terms of area rather than thickness) is unlikely to account for the observed deviation between the experiment and simulation for two reasons. (1) R of the immersed electrode and the new setup were identical at large electrolyte film thicknesses. If the area were not fully covered, R would not have matched. (2) As smaller w (e.g., 250 µm or 500 µm) produce more confined electric fields, insufficient coverage disproportionately affects larger w, where a greater fraction of the electric field extends into the uncovered regions. However, the opposite is observed, where the deviation between experiment and simulation appears more substantial for smaller w.

Secondly, effects of the electrolyte due to evaporation, film thinning, or long measurement times were not observed as each $\alpha(d)$-

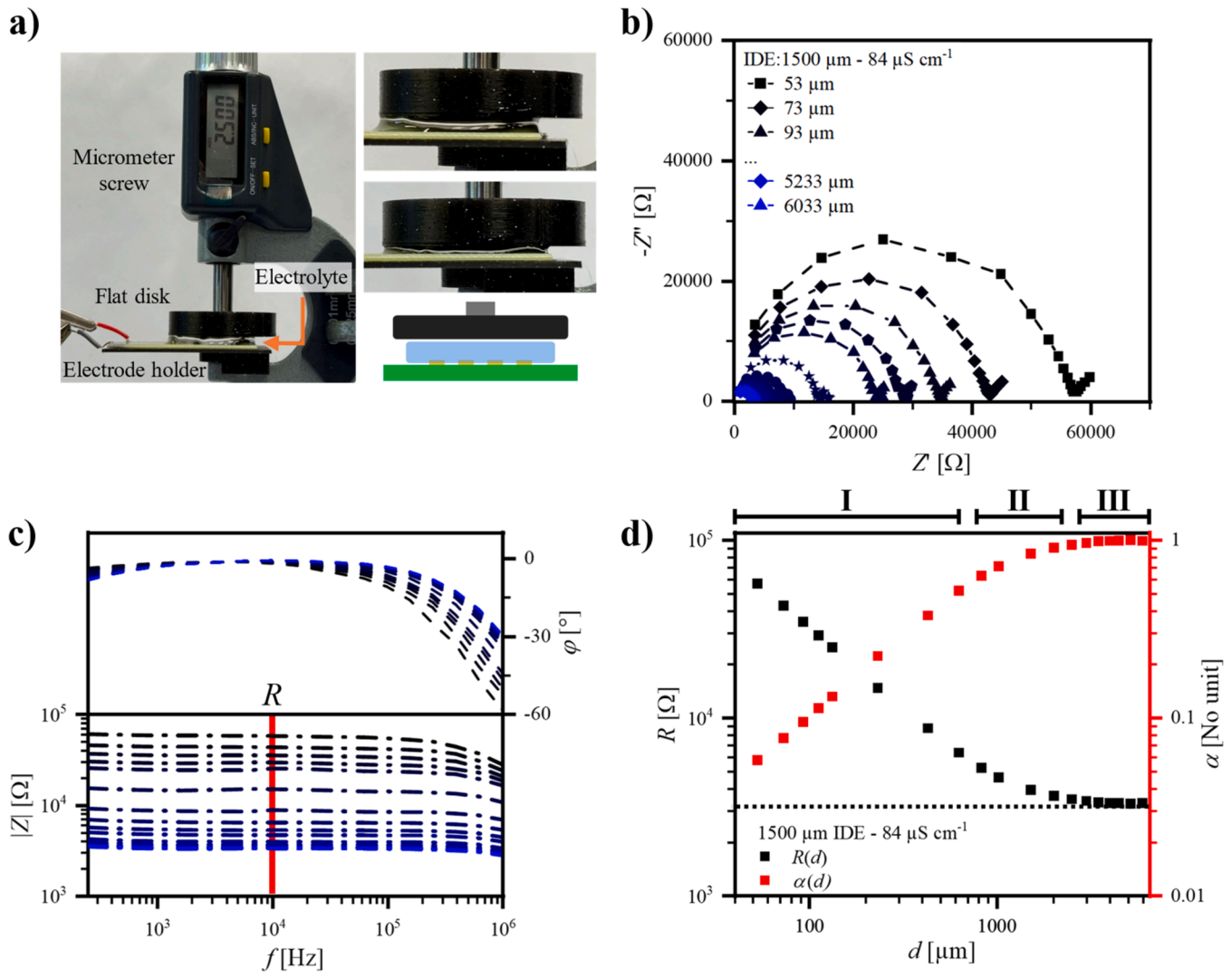

Fig. 3. a) Digital picture of the custom-built setup consisting of a micrometer screw and a tight slip fit flat PLA disk, and an opposing electrode holder. Schematic of the confined electrolyte and electrode and PLA disk surfaces. Capillary forces hold the thin water film between the flat disk and the electrode, and its thickness can be adjusted with the micrometer screw to micrometer precision. Exemplary b) Nyquist and c) Bode plot (Top: φ; Bottom: $|Z|$) of the 1500 µm IDE type for various aqueous electrolyte film thicknesses (53 µm - 6033 µm). d) $R(d)$ (black), and the reciprocally normalized obtained $\alpha(d)$. $R(d)$ at large d converges with R while fully immersed during the k determination (dashed black line). The three regimes of $\alpha(d)$ are indicated above.

determination was completed within <30 min, and the electrolyte was continuously „pressed“ out of the capillary when reducing d, thus preventing local thinning at the capillary edges. Moreover, the PLA disk provided a sufficiently large, wetted area such that any minor thinning would not have reached into the electric field of the electrode. In early experiments performed with DI water, CO_2 uptake was observed throughout the 30 min measurement sequence by the associated gradual acidification and resulting conductivity increase. This affected the extracted $\alpha(d)$, particularly at smaller d (< 500 µm). Although the overall trend remained similar, deviations between successive $\alpha(d)$-determinations on the same electrode were more pronounced. Based on this experience, it is not recommended to determine $\alpha(d)$ over extended time periods or across multiple days.

Lastly, an additional capacitive or conductivity contribution from the PLA disk, as well as an effect caused by the surface roughness of PLA, can be safely excluded. Capacitive contributions were simulated by additionally varying the permittivity (ε) of the air layer (ε: 1-78) with insignificant variations in the simulated current density for all permittivites. Conductive contributions were experimentally investigated by testing different materials (Glass, ABS, Si-Wafer) at various electrolyte concentrations. Any additional conductivity contribution consistently appeared as a conductivity-dominating effect or a partial second or third semicircle within the Nyquist plot. This additional contribution was typically only observed at „low“ electrolyte conductivities (σ < 10 µS cm^{-1}). However, the surface's conductivity contribution was not noticeable for PLA. Lastly, as the PLA disk was fabricated by 3D printing followed by polishing, the topography of the 3D-printed component was probed with confocal laser-scanning microscopy (CLSM, Fig. S3). Although it might seem likely that surface roughness would have a crucial impact on the actual electrolyte film thickness d and thus $\alpha(d)$, differences in observed $\alpha(d)$ for “as-printed” and “polished” PLA disks were insignificant. The polished component had a surface roughness of 20 µm (± 10 µm from the averaged height baseline), along with print line crevices approximately 20 µm wide and 30 µm deep, which were evenly spaced ~500 µm apart. Based on this analysis, it is apparent that the electrolyte film thickness should be unaffected by the component's surface roughness (± 10 µm) at electrolyte film thicknesses much larger (d > 50 µm).

As a final note, our method is intended for „thicker“ films, typically 20 µm - 500 µm, as is commonly found in polymer-composite electrolytes or membranes made of 2D materials, and it is not recommended for very small d (< 20 µm).

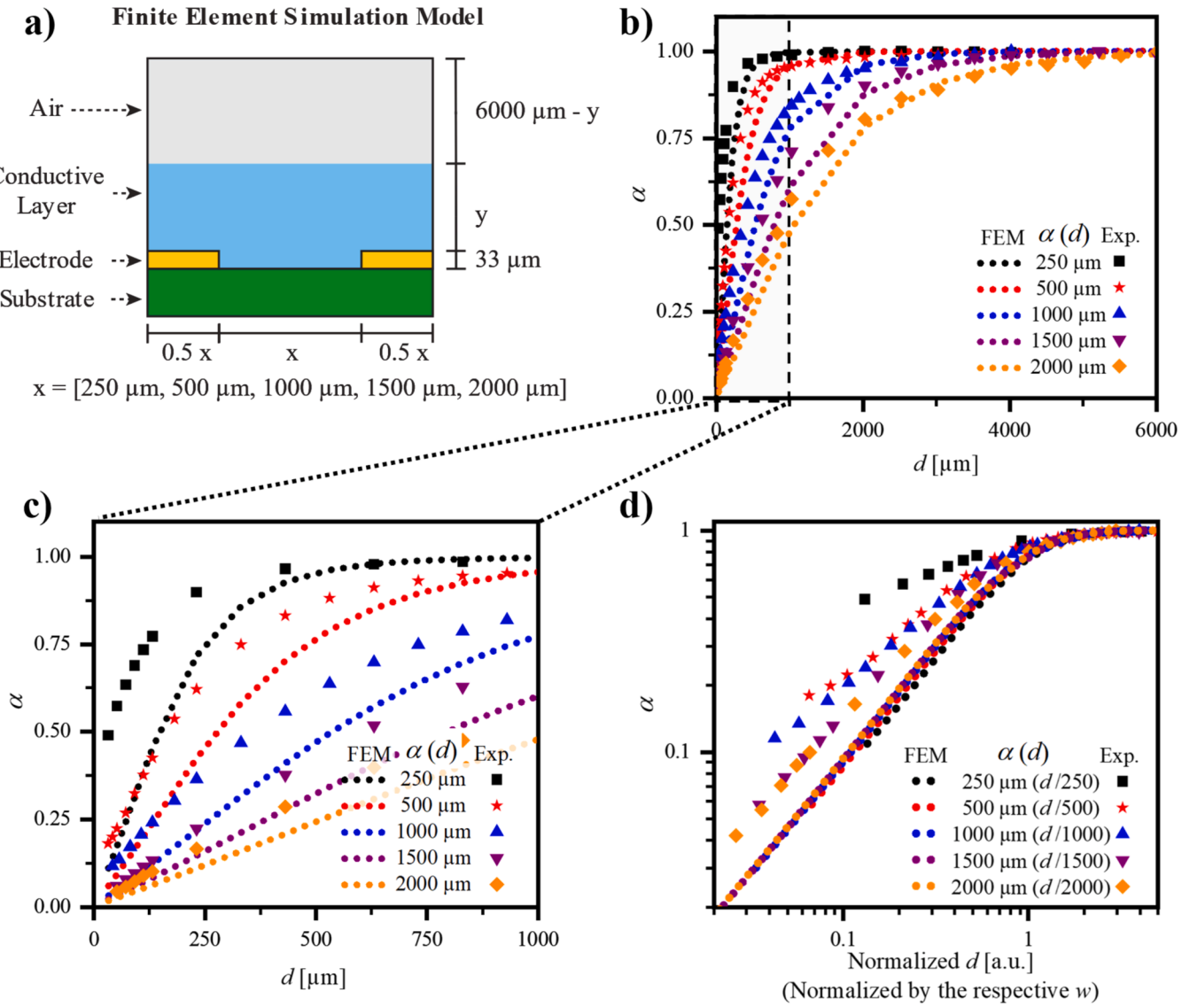

Fig. 4. a) FEM simulation model of the IDE's two-dimensional repeat unit to determine $\alpha(d)$ for thin electrolyte films. Variable parameters were d, w, and s. b) Comparison of the experimental and simulated $\alpha(d)$ of each IDE type (250 µm, 500 µm, 1000 µm, 1500 µm, 2000 µm). c) Expanded view of the experimental and simulated $\alpha(d)$. d) Collapsed datasets of each IDE type's experimental and simulated $\alpha(d)$, by dividing d of each IDE-type by its respective w.

Table 2
L, w & s, N, and k of the smaller array.

Parameter	Dimension
L	5.5 mm
w & s	500 µm
N	8
k	0.347 ± 0.016 cm^{-1}

4. Conclusion

A novel, cost-effective, straightforward procedure was developed to determine the cell constant's correction factor for any IDE as a function of electrolyte film thickness $\alpha(d)$. This method only requires the IDE, a 3D-printed PLA disk, and a micrometer screw. The results were compared to FEM simulations (COMSOL). While the trends of both methods align, the absolute values for $\alpha(d)$ determined experimentally and by FEM simulation differ substantially, particularly at smaller d ($0 < d < 150\ \% * w$). We presume this is due to an oversimplification of the 2D model applied in the simulation, which does not account for the more complex electric field fringes of the array's design. The accuracy of the simulation may be tailored to the electrode by changing the array size. Downsizing the array size increases the accuracy of FEM for small electrolyte film thicknesses ($d < 100\ \% * w$), but decreases the accuracy at larger film thicknesses ($d > 100\ \% * w$). The proposed experimental method for determining $\alpha(d)$ can be expanded to any coplanar electrode geometry, including variations in array size or curved and circular designs. It is only limited by the resolution of the micrometer screw and the precision of the printed components. Overall, these findings highlight the adaptability of interdigitated electrodes and provide a practical framework for tailoring sensor designs to specific material and geometrical constraints. This is a critical step toward enabling next-generation sensor platforms and integrating them across diverse applications, from advanced materials research to environmental monitoring and medical diagnostics. Specifically, it can be used to characterize ionic transport and dielectric behaviour in hydrogel or polymer electrolyte films and nanocomposite coatings.

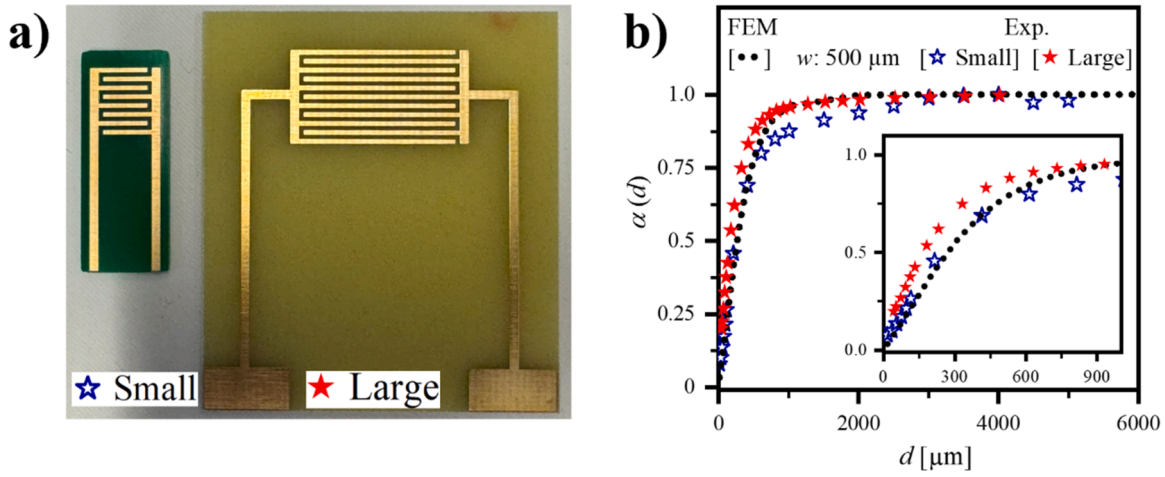

Fig. 5. a) Picture of the small and large IDE-array with identical w, s, and h ($w = s = 500$ µm, and $h = 33$ µm). The dimensions of the large and small array are listed in Tables 1 and 2, respectively. b) Experimental and simulated $\alpha(d)$ of the IDE-arrays.

Statement

During the preparation of this work, the authors used ChatGPT in order to improve readability. After using this tool/service, the authors reviewed and edited the content as needed and take full responsibility for the content of the published article.

CRediT authorship contribution statement

Max Stevenson: Writing – review & editing, Writing – original draft, Visualization, Validation, Software, Methodology, Formal analysis, Data curation, Conceptualization. **Michael König:** Writing – original draft, Software, Data curation. **Ina Klein:** Writing – original draft, Software, Data curation. **Radha Boya:** Writing – review & editing, Writing – original draft, Supervision, Project administration, Conceptualization. **Jürgen Senker:** Writing – review & editing, Supervision. **Markus Retsch:** Writing – review & editing, Supervision. **Josef Breu:** Writing – review & editing, Writing – original draft, Supervision, Project administration, Funding acquisition, Conceptualization.

Declaration of competing interest

The authors declare that they have no known competing financial interests or personal relationships that could have appeared to influence the work reported in this paper.

Acknowledgements and Funding

We gratefully acknowledge the support and funding by the German Research Foundation (DFG) within CRC 1585 (project number 492723217) for subprojects A01, A05, and C05. Support by the BayBatt Cell Technology Center is gratefully acknowledged, which is funded by the Deutsche Forschungsgemeinschaft (DFG, German Research Foundation) – INST 91/452-1 LAGG. We thank Prof. Dr. R. Moos for valuable discussions.

Supplementary materials

Supplementary material associated with this article can be found, in the online version, at doi:10.1016/j.electacta.2025.147985.

Data availability

Data will be made available on request.

References

[1] P. Sun, R. Ma, X. Bai, K. Wang, H. Zhu, T. Sasaki, Single-layer nanosheets with exceptionally high and anisotropic hydroxyl ion conductivity, Sci. Adv. 3 (2017) e1602629, https://doi.org/10.1126/sciadv.1602629.
[2] M.R. Karim, K. Hatakeyama, T. Matsui, H. Takehira, T. Taniguchi, M. Koinuma, Y. Matsumoto, T. Akutagawa, T. Nakamura, S.-i. Noro, T. Yamada, H. Kitagawa, S. Hayami, Graphene oxide nanosheet with high proton conductivity, J. Am. Chem. Soc. 135 (2013) 8097–8100, https://doi.org/10.1021/ja401060q.
[3] M. Stevenson, S. Pappler, L. Kanzler, A. Nisar, J.K. Parambath, M. Rosenstihl, F. Lebeda, S. Weiß, G. Papastavrou, M. Vogel, J. Senker, J. Breu, Ion and Solvent dynamics in charged 2D clay nanoslits with unprecedented ångström-precise slit height control, Adv. Funct. Mater. (2025) e15706, https://doi.org/10.1002/adfm.202515706.
[4] S. Joo, J.Y. Han, S. Seo, J.-H. Kim, Patterning techniques in Coplanar Micro/Nano capacitive sensors, Micromach 14 (2023) 2034, https://doi.org/10.3390/mi14112034.
[5] H. Cui, X. Xiong, B. Gao, Z. Chen, Y. Luo, F. He, S. Deng, L. Chen, A novel impedimetric biosensor for detection of lead(II) with low-cost interdigitated electrodes made on PCB, Electroanalysis 28 (2016) 2000–2006, https://doi.org/10.1002/elan.201501153.
[6] S. Habboush, S. Rojas, N. Rodríguez, A. Rivadeneyra, The role of interdigitated electrodes in printed and flexible electronics, Sensors 24 (2024) 2717, https://doi.org/10.3390/s24092717.
[7] G.J.A.M. Brom-Verheijden, M.H. Goedbloed, M.A.G. Zevenbergen, A microfabricated 4-electrode conductivity sensor with enhanced range, Proceedings 2 (2018) 797, https://doi.org/10.3390/proceedings2130797.
[8] W. Olthuis, W. Streekstra, P. Bergveld, Theoretical and experimental determination of cell constants of planar-interdigitated electrolyte conductivity sensors, Sens. Actuat. B: Chem. 24 (1995) 252–256, https://doi.org/10.1016/0925-4005(95)85053-8.
[9] D. Sharon, P. Bennington, C. Liu, Y. Kambe, B.X. Dong, V.F. Burnett, M. Dolejsi, G. Grocke, S.N. Patel, P.F. Nealey, Interrogation of electrochemical properties of polymer electrolyte thin films with interdigitated electrodes, J. Electrochem. Soc. 165 (2018) H1028, https://doi.org/10.1149/2.0291816jes.
[10] M. Daab, P. Loch, W. Milius, D. Schönauer-Kamin, M. Schubert, A. Wunder, R. Moos, F.E. Wagner, J. Breu, Single-crystal structure and electronic conductivity of melt synthesized Fe-rich, near end-member ferro-kinoshitalite, Z. Anorg. Allg. Chem. 643 (2017) 1661–1667, https://doi.org/10.1002/zaac.201700265.
[11] A. Javed, T. Wagner, S. Wöhlbrandt, N. Stock, M. Tiemann, Proton conduction in a single crystal of a phosphonato-sulfonate-based coordination polymer: mechanistic insight, ChemPhysChem 21 (2020) 605–609, https://doi.org/10.1002/cphc.202000102.
[12] D. Berdat, A.C. Martin Rodríguez, F. Herrera, M.A.M. Gijs, Label-free detection of DNA with interdigitated micro-electrodes in a fluidic cell, Lab. Chip. 8 (2008) 302–308, https://doi.org/10.1039/B712609C.
[13] F. Vahidpour, Y. Alghazali, S. Akca, G. Hommes, M.J. Schöning, An enzyme-based interdigitated electrode-type biosensor for detecting low concentrations of H2O2 vapor/aerosol, Chemosensors 10 (2022) 202, https://doi.org/10.3390/chemosensors10060202.
[14] R. de la Rica, C. Fernández-Sánchez, A. Baldi, Polysilicon interdigitated electrodes as impedimetric sensors, Electrochem. Commun. 8 (2006) 1239–1244, https://doi.org/10.1016/j.elecom.2006.05.028.
[15] L.E. Delle, V. Pachauri, A. Vlandas, M. Riedel, B. Lägel, R. Lilischkis, X.T. Vu, P. Wagner, R. Thoelen, F. Lisdat, S. Ingebrandt, Scalable fabrication and application of nanoscale IDE-arrays as multi-electrode platform for label-free biosensing, Sens. Actuat. B: Chem. 265 (2018) 115–125, https://doi.org/10.1016/j.snb.2018.02.174.

[16] A.E. Cohen, R.R. Kunz, Large-area interdigitated array microelectrodes for electrochemical sensing, Sens. Actuat. B: Chem. 62 (2000) 23–29, https://doi.org/10.1016/S0925-4005(99)00372-X.
[17] S. Calvi, L. Basiricò, S.M. Carturan, I. Fratelli, A. Valletta, A. Aloisio, S. De Rosa, F. Pino, M. Campajola, A. Ciavatti, L. Tortora, M. Rapisarda, S. Moretto, M. Verdi, S. Bertoldo, O. Cesarini, P. Di Meo, M. Chiari, F. Tommasino, E. Sarnelli, L. Mariucci, P. Branchini, A. Quaranta, B. Fraboni, Flexible fully organic indirect detector for megaelectronvolts proton beams, npj Flex. Electron. 7 (2023) 5, https://doi.org/10.1038/s41528-022-00229-w.
[18] J. Exner, R. Moos, Ermittlung spezifischer Materialkennwerte von Schichten mittels Interdigital-Elektroden, in: *12. Dresdner Sensor-Symposium 2015*, 2015, pp. 256–259, https://doi.org/10.5162/12dss2015/P7.10.